Acoustic Emission Characteristics of Mode I Rock Fracturing

Arthur D. De Alwis, Mehdi Serati
School of Civil Engineering, The University of Queensland, Brisbane, Australia

Derek Martin
Faculty of Civil Engineering, The University of Alberta, Edmonton, Canada

Arcady Dyskin
School of Engineering, The University of Western Australia, Perth, Australia

Elena Pasternak
School of Engineering, The University of Western Australia, Perth, Australia

David J. Williams
School of Civil Engineering, The University of Queensland, Brisbane, Australia

ABSTRACT: Understanding the propagation of Mode I fracture is crucial in rock mechanics since this fracture mode is the predominant cause of catastrophic failures in brittle rock-like solids. For investigating the mechanisms of rock fracturing, Acoustic Emission (AE) is a widely accepted tool. In this paper, various AE parameters, including the number of hits, source location, Rise Angle (RA), and Average Frequency (AF) are considered to evaluate the AE characteristics during Mode I loading-induced fracturing of basalt. Certain waveform features such as the dominant frequency and amplitude distribution are further investigated. Results suggest interesting findings in the changes in cumulative hits, source location, and RA at different stages of fracture. The observed trend in peak frequencies found in the study, in particular, points to promising future studies.

Keywords: Mode I Rock Fracture, Acoustic Emission, Source Location, Rise Angle, Average Frequency, Dominant Frequency.

1 INTRODUCTION

Fracture propagation in brittle rocks is predominantly Mode I, unless there exist pre-existing weak surfaces directing the propagating fractures, e.g. as discussed in detail by Fairhurst and Cook (1966) and Germanovich, et al. (1994). To capture the failure of rocks at different stress regimes and failure modes, including Mode I, Acoustic Emission (AE) has been used extensively in the literature (Manthei et al., 2022). Recorded AE events can be evaluated through parametric analysis or quantitative/waveform analysis. Several studies of rock fracturing have used AE measurements in Cracked Chevron Notched Brazilian Disc (CCNBD) specimens or Semi-Circular Bending (SCB) tests (Aggelis et al., 2013; Guo & Wong, 2021; Guo & Zhao, 2022; Nasseri et al., 2006; Yang et al., 2022). However, the Rise Angle (RA) versus the Average Frequency (AF) relationship during fracture evolution has been largely underutilized. To address this gap, CCNBD specimens were preferred in this work to evaluate Mode I fracture of basalt, considering that CCNBD specimen testing is well-established to obtain Mode I fracture toughness (Serati et al., 2016). Basalt was also selected as the preferred rock type since basaltic rock formations have served as foundations for several civil infrastructure projects in Australia and worldwide (Jain et al., 2014); including Baihetan, Xiluodu and Tongjiezi hydropower stations (Xia et al., 2020), the transfer tunnel of Kaste dam in

Lesotho, South Africa (Bell & Haskins, 1997), and in the petroleum industry where oil deposits have been discovered in and around basaltic deposits (Huang et al., 2019).

2 METHODOLOGY

This study analyzed Mode I fracture propagation in two basalt specimens, B01 and B02, using the ISRM CCNBD specimens (Fowell et al., 1995). To make the Chevron notch, a milling machine was used with a blade attached to the chuck of the milling machine, and the required displacement was achieved by moving the sample towards the blade. Specimens were oven dried at 105° C after the Chevron notches were made. Tables 1 and 2 provide the mechanical properties, dimensions, and measured fracture toughness for the selected specimens.

Table 1. Basalt mechanical properties.

Parameters		Value
Modulus of elasticity	GPa	45.42 ±3.74
Poison's ratio		0.24±0.01
Dry density	kg/m^3	2,577±13.05
Porosity	%	7.15±0.16
Uniaxial Compressive Strength (UCS)	MPa	131±3.5
P-wave velocity	m/s	4,739 ± 23.47

Figure 1a illustrates the schematics of the tests. Specimens were tested using a 100 kN Instron 4505 loading frame. The low loading rate of 2kN/m, less than the one suggested by Fowell et al. (1995) was chosen to better visualize the fracturing events during the AE data acquisition stage and to ensure that synchronization between the loading and AE system was optimized. Ten (10) Mistras Physical Acoustics AE sensors (WD-type) with operational frequencies from 100 kHz to 1,000 kHz were used. The preamplifier type used was a PreAmp One 5V model with a preamplification of 26 dB. The data acquisition (DAQ) system consisted of the two express 8 cards, which recorded the waveforms at 16-bit resolution. The waveforms were recorded at a 5 MHz sampling rate. Tests were carried out with Automatic Sensor Testing (AST) configuration, an inbuilt function of the AE system where the sensors send pulses in a sequence and capture the arrival time of the pulses generated. The AST was set to generate five pulses and we selected the minimum threshold at which all the pulses were captured by each sensor, which was found to be 50dB. The minimum threshold was selected to capture the relevant AE characteristics and to filter noise. Mistras Physical Acoustics "AE Win" software was adopted to post-process and acquire AE information. The arrangement of the sensors is shown in Figure 1b. Only a 2D analysis of the source location was conducted within the fracture plane (see also Figure 1a).

Table 2. Dimensions and Mode I fracture toughness of the Basalt specimens.

Specimen	D(mm)	B(mm)	D_s(mm)	a_0(mm)	a_1(mm)	h_c(mm)	P_{max}(kN)	Y^*_m	K_{IC}(MPa√m)
B01	99.52	35.64	76	14.02	33.73	20.5	17.3	0.90	1.39
B02	99.35	38.18	76	10.26	33.73	20.5	18.26	0.87	1.32
Average	99.44	36.91	-	12.14	-	-	17.78	-	1.35
St. Dev.	0.085	1.27	-	1.88	-	-	0.48	-	0.03

3 RESULTS

The number of hits is a basic characteristic of AE studies (Moradian et al., 2015; Goodfellow et al., 2015). The AE counts together with the applied load vs. time plots are shown in Figure 2. It can be seen that despite the same loading arrangements for both tests, the AE counts, the time of AE commencement, and the start of fracture propagation are different. Furthermore, the counts have ups and downs, which are different for the two specimens. This is likely due to rock variability: different specimens of the same rock can behave differently. To further investigate the evolution of fracture growth, we considered the propagation of source location and how the waveform features change

with fracture propagation. The failure load was divided into four parts (in % of the maximum force): < 95%, 95–98%, 98–99% and 99–100%. The events were considered if six or more channels were triggered (crossed the threshold limit).

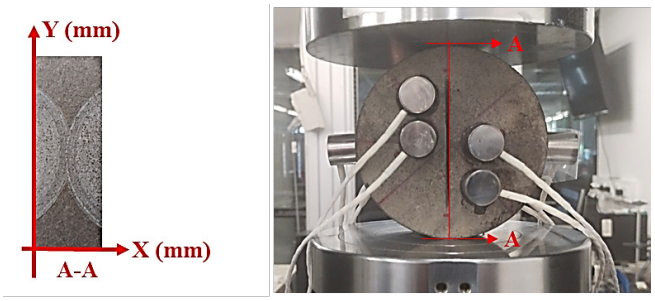

(a) (b)

Figure 1. Schematics of the experiment: (a) the CCNBD basalt samples; (b) the positions of the AE sensors.

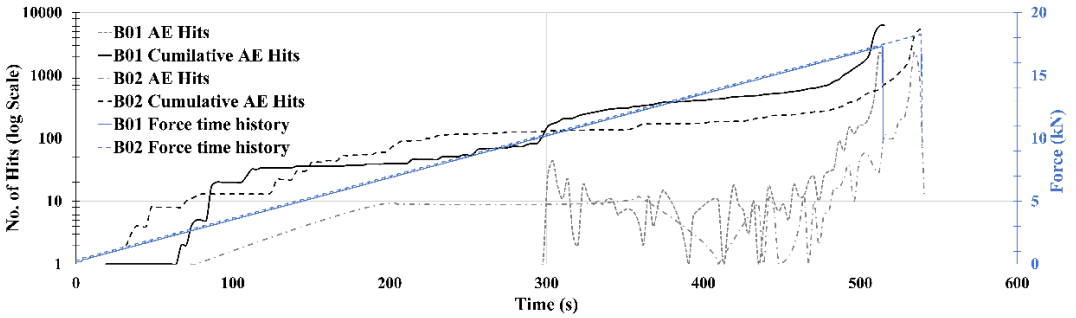

Figure 2. Registered and cumulative AE hits (counts) vs. time and the force-time history.

For source location, a total of 10 sensors were used. But, it should be noted due to the Chevron notch being in the middle of the specimens the waves may be attenuated, hence not all 10 channels may be triggered. Therefore a minimum of six sensors were chosen to be triggered as a criterion for recording the signal. We selected the analysis plane to be at the centre of the predefined Chevron notch (Figure 1) and the location of the microfracture sources was divided based on the normalized failure load. Figure 3, illustrates the new source locations at different normalized force levels, while the previous events are greyed out. It is noted that some of the events occur in the seemingly empty space (where the predefined crack exists). However, this could be attributed to the limited precision of the procedure of source location, such that secondary fractures are detected. One should not exclude bridge formation in the process of fracture propagation, (He et al., 2020); the bridges then break producing AE signals. Figure 3 also shows that most events occur at the final stages of loading i.e., at the 99-100% band, which could be due to the initiation of unstable fracture growth causing a significant increase in the AE events. The microfracture source locations are randomly scattered (one would expect more fractures to occur at the notch tip and progress toward the boundary as the fracture propagates). This was also noted in the study by Kaklis et al. (2017) on marble samples.

Aggelis and Shiotani (2022) described the application of two of the waveform parameters used to classify the fracture mode, which are the Rise Angle (RA) and the Average Frequency (AF). The use of RA vs. AF plots has also been extended to classify the microfracture of different types of rocks such as granite, sandstone, dolomite, marble, shale etc. (Li et al., 2018; Wang et al., 2017; Zhang et al., 2022; Zhang & Deng, 2020). RA is defined as the ratio between the time at which the maximum amplitude is reached (often defined as the rise time) and the maximum amplitude, while AF is defined as the ratio between the number of hits and the duration of the recorded waveform as illustrated in Figure 4. The RA vs. AF plots with increasing load are shown in Figure 5. Figure 6d shows that high RA (low AF) events were generated during the last stage of fracturing.

Zhang and Deng (2020) used the rationale of low-frequency bandwidth to be associated with tensile events, and high-frequency events to be associated with shear events, and used these correlations to optimize the transition line of RA vs. AF plots, to differentiate tensile and shear

events. Interestingly, most of the events occurred at a relatively lower amplitude range in both cases. Low to high-amplitude signals were observed in both the low and high-frequency bandwidths. It can also be noted that there are clear frequency bands that have been formed between 100 kHz and 300 kHz and 400k KHz and 600 kHz with very minimal peak frequencies in the range 300 kHz and 400 kHz in the B01 specimen as shown in Figure 6. Li et al. (2017) and Zhang and Deng (2020) associated the lower band frequencies with tensile fractures, while higher band frequencies were associated with shear fractures.

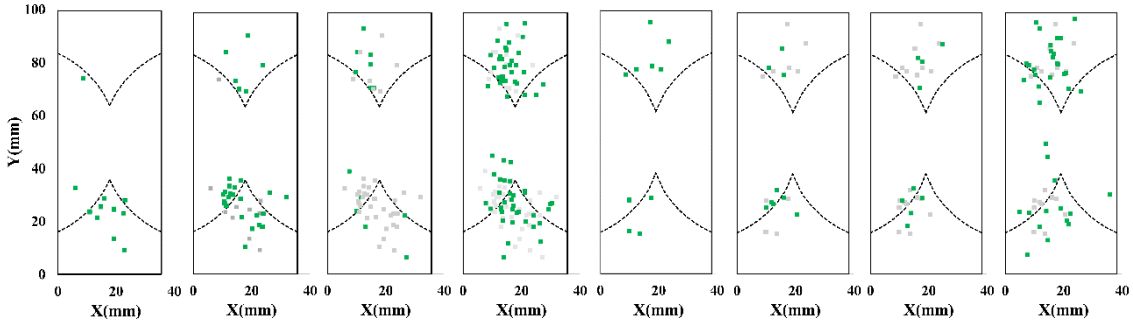

Figure 3. Source location of basalt specimens with different normalized Mode I failure load levels (a) <95% $P_{Max\text{-}B01}$, (b) 95-98% $P_{Max\text{-}B01}$, (c) 98-99% $P_{Max\text{-}B01}$, (d) 99-100% $P_{Max\text{-}B01}$, (e) <95% $P_{Max\text{-}B02}$, (f) 95-98% $P_{Max\text{-}B02}$, (g) 98-99% $P_{Max\text{-}B02}$, (h) 99-100% $P_{Max\text{-}B02}$.

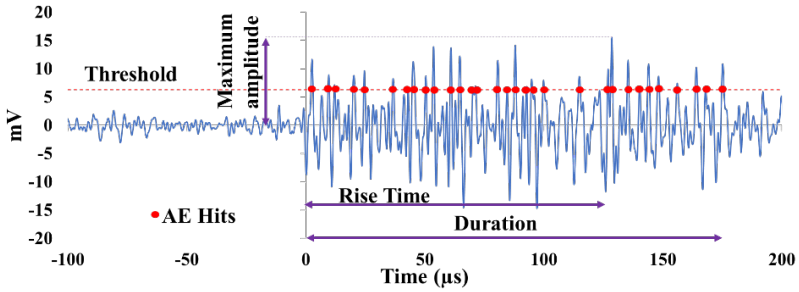

Figure 4. Illustration of AE parameters.

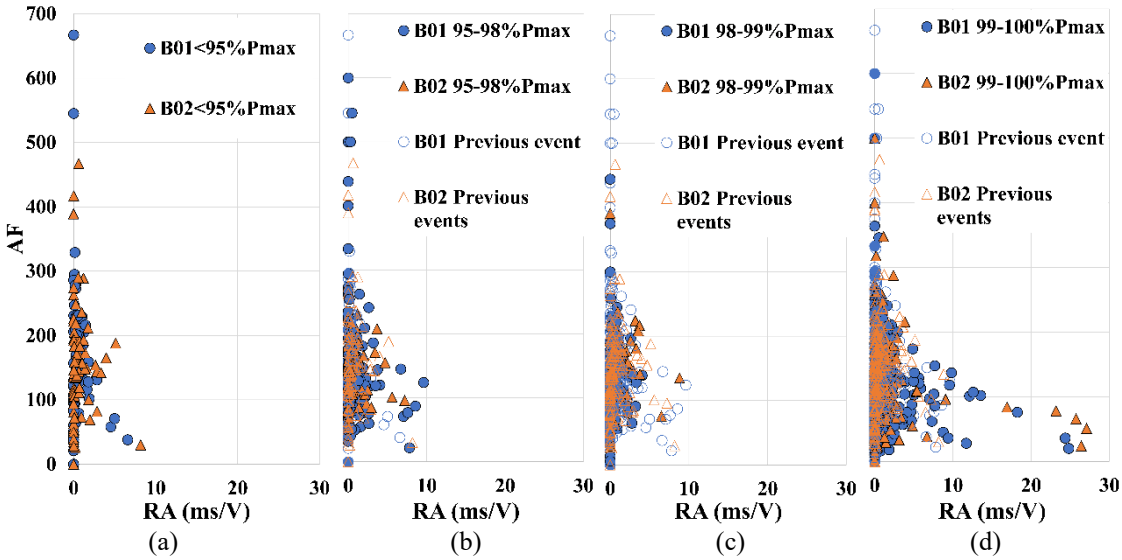

Figure 5. Variation of RA vs AF plot with increasing load (a) <95% P_{Max}, (b) 95-98% P_{Max}, (c) 98-99% P_{Max}, (d) 99-100% P_{Max}.

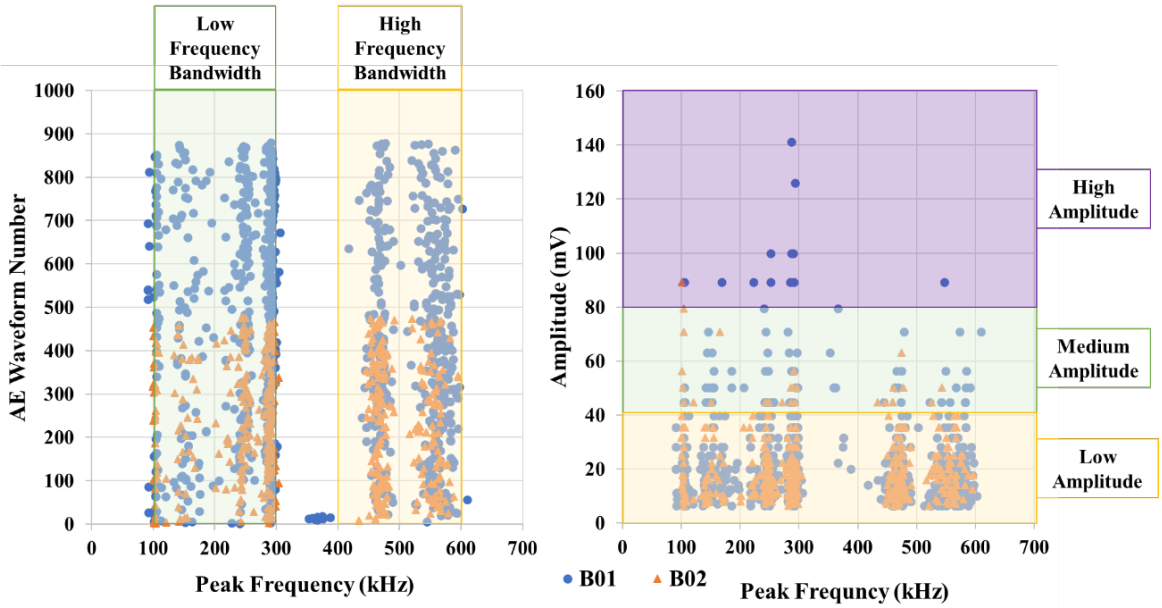

(a) (b)

Figure 6. Frequency analysis: (a) peak frequency distribution; (b) peak frequency vs. amplitude, the transition lines run at amplitudes 40 and 80 (mV).

4 CONCLUSIONS

Tested basalt specimens in this study demonstrate rock variability: two specimens of the same rock loaded at the same rate exhibit a considerable difference in AE counts and fracture loads. The analysis of the AE characteristics of the two specimens during fracture propagation showed an increase in the number of hits and cumulative hits at around 95% of the maximum failure load. Secondary fractures were observed in the specimens, and source location analysis indicated events within the apparent fracture space, which were assumed to be associated with the secondary fractures. The RA vs. AF graph was used to reflect the four stages of fracture defined by the normalized maximum Mode I fracture failure load. It was noted that extreme RA (with low AF) waveforms were generated during the last stage of fracturing. The peak frequencies indicated the existence of two frequency bandwidths, and a significant amount of lower amplitude waves were observed in both specimens.

ACKNOWLEDGEMENTS

The authors acknowledge support from the Australian Research Council through Discovery Project DP210102224. The authors thank Jiangwan He for measuring the Basalt properties.

REFERENCES

Aggelis, D., Mpalaskas, A., & Matikas, T. (2013). Investigation of different fracture modes in cement-based materials by acoustic emission. *Cement and Concrete Research*, *48*, 1-8.

Aggelis, D. G., & Shiotani, T. (2022). Parameters Based AE Analysis. In *Acoustic Emission Testing* (2 ed., pp. 45-71). Springer.

Bell, F., & Haskins, D. (1997). A geotechnical overview of Katse Dam and Transfer Tunnel, Lesotho, with a note on basalt durability. *Engineering Geology*, 46(2), 175-198.

Fairhurst, C. & Cook, N.G.W. (1966). The phenomenon of rock splitting parallel to the direction of maximum compression in the neighbourhood of a surface. *Proc. First Congr. Intern. Soc Rock Mech.*, Lisbon, **1**, 687-692.

Fowell, R., Hudson, J., Xu, C., & Zhao, X. (1995). Suggested method for determining Mode I fracture toughness using Cracked Chevron Notched Brazilian disc (CCNBD) specimens. Intern. J. Rock Mech. and Mining Sci. , Vol. 32, No. I, pp. 57--64, 1995

Germanovich, L.N., Salganik, R.L., Dyskin, A.V. & Lee, K.K. 1994. Mechanisms of brittle fracture of rock with multiple pre-existing cracks in compression. *Pure and Applied Geophysics*, 143, 117-149.

Goodfellow, S., Tisato, N., Ghofranitabari, M., Nasseri, M., & Young, R. (2015). Attenuation properties of Fontainebleau sandstone during true-triaxial deformation using active and passive ultrasonics. *Rock Mech. and Rock Eng.*, *48*(6), 2551-2566.

Guo, T. Y., & Wong, L. N. Y. (2021). Cracking mechanisms of a medium-grained granite under mixed-mode I-II loading illuminated by acoustic emission. *Intern. J. Rock Mech. and Mining Sci.*, *145*, 104852.

Guo, T. Y., & Zhao, Q. (2022). Acoustic Emission Characteristics During the Microcracking Processes of Granite, Marble and Sandstone Under Mode I Loading. *Rock Mech. and Rock Engineering*, 1-23.

He, J., Pasternak, E., Dyskin, A.V. 2020. Bridges outside fracture process zone: Their existence and effect. *Engineering Fracture Mechanics,* 225, 106453.

Huang, Y., Leng, Q., Zhao, J., & Wang, S. (2019). Hydrocarbon Accumulations in and around Basalts in the Cenozoic of Northeast Bohai Bay Basin, China. In: 2019 AAPG Annual Convention and Exhibition.

Ishida, T., Labuz, J. F., Manthei, G., Meredith, P. G., Nasseri, M., Shin, K., Yokoyama, T., & Zang, A. (2017). ISRM suggested method for laboratory acoustic emission monitoring. *Rock Mech. and Rock Eng.*, 50, 665-674.

Jain, P., Naithani, A., & Singh, T. (2014). Performance characteristics of tunnel boring machine in basalt and pyroclastic rocks of Deccan traps–A case study. *J. Rock Mech. and Geotechnical Eng.*, *6*(1), 36-47.

Kaklis, K., Mavrigiannakis, S., Saltas, V., Vallianatos, F., & Agioutantis, Z. (2017). Using acoustic emissions to enhance fracture toughness calculations for CCNBD marble specimens. *Frattura ed Integrità Strutturale*, *11*(40), 1-17.

Li, L., Deng, J., Zheng, L., & Liu, J. (2017). Dominant frequency characteristics of acoustic emissions in white marble during direct tensile tests. *Rock Mechanics and Rock Engineering*, *50*(5), 1337-1346.

Li, Z., Wang, L., Lu, Y., Li, W., & Wang, K. (2018). Experimental investigation on the deformation, strength, and acoustic emission characteristics of sandstone under true triaxial compression. *Advances in Materials Science and Engineering*, Article ID 5241386, 16 pages,.*2018*.

Manthei, G., Zang, A., & Grosse, C. U. (2022). Laboratory Acoustic Emission in Study of Rock Mechanics. In *Acoustic Emission Testing* (2 ed., pp. 477-527). Springer.

Moradian, Z., Einstein, H. H., & Ballivy, G. (2015). Detection of cracking levels in brittle rocks by parametric analysis of the acoustic emission signals. *Rock Mechanics and Rock Engineering*, *49*(3), 785-800.

Nasseri, M., Mohanty, B., & Young, R. (2006). Fracture toughness measurements and acoustic emission activity in brittle rocks. *Pure and Applied Geophysics*, *163*(5), 917-945.

Serati, M., Alehossein, H., & Erarslan, N. (2016). The Brazilian disc test under a non-uniform contact pressure along its thickness. Rock Mechanics and Rock Engineering, 49, 1573-1577.

Wang, M., Tan, C., Meng, J., Yang, B., & Li, Y. (2017). Crack classification and evolution in anisotropic shale during cyclic loading tests by acoustic emission. *J. Geophysics and Engineering*, *14*(4), 930-938.

Xia, Y., Zhang, C., Zhou, H., Chen, J., Gao, Y., Liu, N., & Chen, P. (2020). Structural characteristics of columnar jointed basalt in drainage tunnel of Baihetan hydropower station and its influence on the behaviour of P-wave anisotropy. *Engineering Geology*, *264*, 105304.

Yang, Z., Yin, T., Zhuang, D., Wu, Y., Yin, J., & Chen, Y. (2022). Effect of temperature on mixed Mode I/III fracture behaviour of diorite: An experimental investigation. *Theoretical and Applied Fracture Mechanics*, 103571.

Zhang, X., Li, Z., Wang, X., Wang, H., Li, B., & Niu, Y. (2022). Thermal effect on the fracture behaviour of granite using acoustic emission and digital image correlation: an experimental investigation. *Theoretical and Applied Fracture Mechanics*,122, 103571.

Zhang, Z.-H., & Deng, J.-H. (2020). A new method for determining the crack classification criterion in acoustic emission parameter analysis. *Intern. J. Rock Mechanics and Mining Sci.*, *130*, 104323.